

Triplet character of 2D-fermion dimers arising from s -wave attraction via spin-orbit coupling and Zeeman splitting

Ulrich Ebling¹, Ulrich Zülicke² and Joachim Brand^{1*}

¹ Dodd-Walls Centre for Photonic and Quantum Technologies, Centre for Theoretical Chemistry and Physics, New Zealand Institute for Advanced Study, Massey University, Private Bag 902104, North Shore, Auckland 0745, New Zealand

² Dodd-Walls Centre for Photonic and Quantum Technologies, School of Chemical and Physical Sciences, Victoria University of Wellington, PO Box 600, Wellington 6140, New Zealand

* j.brand@massey.ac.nz

December 20, 2021

Abstract

We theoretically study spin-1/2 fermions confined to two spatial dimensions and experiencing isotropic short-range attraction in the presence of both spin-orbit coupling and Zeeman spin splitting – a prototypical system for developing topological superfluidity in the many-body sector. Exact solutions for two-particle bound states are found to have a triplet character that can become dominant in the regime of weak attractive s -wave interaction when the energy scale of spin-orbit coupling is comparable to a combination of the Zeeman and center-of-mass kinetic energies. The center-of-mass momentum is one of the parameters determining the existence of bound states, which we map out for both two- and one-dimensional types of spin-orbit coupling. Distinctive features emerging in the orbital part of the bound-state wave function, including but not limited to its p -wave character, provide observable signatures of unconventional pairing.

Contents

1	Introduction	2
2	General formalism for solving the two-particle problem	4
2.1	Case of noninteracting particles	5
2.2	Bound states resulting from s -wave attraction	6
2.3	Binding energy from the Bethe-Peierls boundary condition	8
3	Bound-state properties for 2D-type spin-orbit coupling	9
3.1	Case of zero center-of-mass momentum	9
3.2	Effect of finite center-of-mass momentum	11
4	Bound states formed with 1D-type spin-orbit coupling	13
5	Orbital characteristics of the bound-state wave function	14

6	Experimental detection	15
7	Conclusions and outlook	15
A	Singlet- and triplet-state projections of helicity product states	16
B	Momentum representation of the Green's function	17
C	Boundary of parameter region where a $P = 0$ bound state exists	18
D	Fractional weight of total-spin eigenstates in $P = 0$ bound states	19
	References	19

1 Introduction

Since their early days, ultracold atomic gases have provided an intriguing avenue for exploring and simulating condensed-matter-physics phenomena. Artificial gauge fields [1–4] constitute pertinent examples for the great degree of control and ability to fine-tune parameters that are often fixed in a solid-state material. While spin-orbit coupling for quasi-free electrons in materials is fundamentally determined by the band structure [5–8] and can only be manipulated in a limited fashion via nanostructuring [9], it has recently become possible to realize synthetic versions of one-dimensional (1D) [1] and two-dimensional (2D) [10, 11] types of spin-orbit coupling for ultracold neutral atoms by means of Raman coupling with lasers. Furthermore, advances in manipulating and probing quantum gases have enabled the study of low-dimensional systems such as 2D Fermi gases [12–19] and provided detailed insights into their many-body physics via spectroscopic techniques [20]. In the future, low-dimensional systems with spin-orbit coupling and Zeeman spin splitting will allow experimentalists to create exotic condensed-matter phases such as topological superfluids that can host unconventional Majorana-fermion excitations [21]. Mean-field theory predicts the emergence of such a topological phase in s -wave superfluids of 2D fermions with spin-orbit coupling and large-enough Zeeman splitting [22–26].

Complementary to mean-field studies of interacting many-particle systems, analysis of the two-fermion bound state in vacuum sheds a different light on pairing that can provide crucial insight, e.g., into the strong-coupling (BEC) limit of tightly bound dimers. Dimers of fermionic atoms are further of interest in their own right, e.g., as providing qubits for quantum information processing [27]. We consider two particles (atoms) interacting only via isotropic, short range, and attractive low-energy s -wave scattering under the influence of synthetic spin-orbit coupling. Previous work on bound states in 3D [28–31] (see Ref. [32] for a trapped system) and in 2D [33–35] largely ignored the effects of Zeeman spin splitting. Dimers of spin-orbit-coupled fermions in a 3D gas have already been produced and probed experimentally [36].

The presence of spin-orbit coupling adds several interesting features to the two-particle problem, including the fact that strongly bound states acquire properties solely determined by the gauge field (becoming so-called "rashbons" [29]). Furthermore, Galilean invariance is broken. While total center-of-mass (COM) momentum is still conserved, it enters the bound-state problem

as a parameter. As a consequence, bound states may dissociate when scattered to large values of the COM momentum [29, 35]. Also, spin-orbit coupling induces a spin-triplet component in the two-fermion bound state even with pure s -wave attraction [28, 33, 36]. This is in contrast to the situation in the absence of spin-orbit coupling, where s -wave attraction has no effect in the decoupled triplet channel and, thus, generates pure spin-singlet bound states (including in situations with Zeeman splitting present [36, 37]). As s -wave interactions are usually dominant in ultracold atoms where higher-orbital-momentum interactions are strongly suppressed [38], spin-orbit coupling is thus a promising avenue to induce a triplet character to atomic dimers.

In this paper, we examine the exact bound-state solutions of the two-particle Schrödinger equation in 2D. By considering the effects of Zeeman spin splitting on the same footing as finite COM momentum, we extend previous works where the effects of Zeeman spin splitting were not considered in detail [33–35]. We calculate the dimer bound-state energy and delineate the critical boundary in parameter space beyond which Zeeman splitting and/or COM momentum destabilise the bound state. We also calculate, for the first time, the spin projections for the 2D bound states. The orbital part of the bound-state wave function projected onto spin-singlet and -triplet components reveals their respective s -wave and p -wave-like features. We find that both finite COM momentum and Zeeman spin-splitting favour triplet contributions to the ground state and contribute similar effects to the bound-state problem. However, while finite COM momentum favours unpolarised triplet character, the Zeeman spin splitting leads to a spin-polarised triplet character of the bound state that is associated with a chiral- p -wave orbital wave function. Such triplet-dominated p -wave dimers can be seen as a precursor of the topological superfluid that is expected to emerge in the many-body regime [21, 22, 26]. The region in parameter space where the triplet character dominates turns out to be a striking feature of systems with 2D-type (e.g., Rashba [39–41]) spin-orbit coupling, but triplet-dominated bound states are also present for 1D-type spin-orbit coupling, albeit in a reduced parameter range.

The remainder of this paper is organized as follows. In section 2, we develop the general formalism for solving the two-particle problem for any type of spin-orbit coupling and an effective Zeeman splitting that subsumes both the actual Zeeman spin splitting and finite COM momentum. In section 3, we apply this formalism to obtain bound-state solutions for 2D-type spin-orbit coupling. We first discuss the case with zero COM momentum where we obtain analytic expressions for all terms in the implicit equation for the bound-state energy as well as for the critical value of the Zeeman-spin-splitting energy above which no bound state exists. We also calculate the relative weights of spin-singlet and spin-triplet components in the two-fermion bound state and find that a parameter region exists where bound dimers have a large triplet component. We then address the case of finite COM momentum, for which no analytical results can be obtained and where the shape of the bound state is different. In section 4, we repeat our analysis for the case of 1D-type spin-orbit coupling. Compared with the 2D-type spin-orbit coupling, the parameter range for having a bound state is increased. In contrast, while bound states with a dominant triplet component still exist in this case, the interaction strength needs to be tuned to considerably weaker magnitudes compared to the 2D-type spin-orbit-coupling case to find those states. Then, in section 5, we plot the orbital part of the bound-state wave function in relative-momentum space for the different total-spin components and parameter regimes considered in the preceding sections. We discuss possible experimental detection methods in section 6 before presenting our conclusions in section 7.

Table 1: Types of spin-orbit coupling considered in this work. Each of these is associated with a particular form of the term $\hat{\lambda}(\mathbf{p})$ in the single-particle Hamiltonian (2) and with a matrix \mathcal{M} entering the transformation of momentum vectors via Eq. (3). The constant λ , which has dimensions of velocity, quantifies the magnitude of the spin-orbit coupling.

	2D-Dirac	2D-Rashba	2D-Dresselhaus	1D
$\hat{\lambda}(\mathbf{p})$	$\lambda(p_x \hat{\sigma}_x + p_y \hat{\sigma}_y)$	$\lambda(p_y \hat{\sigma}_x - p_x \hat{\sigma}_y)$	$\lambda(p_x \hat{\sigma}_x - p_y \hat{\sigma}_y)$	$\lambda p_x \hat{\sigma}_x$
\mathcal{M}	$\begin{pmatrix} 1 & 0 \\ 0 & 1 \\ 0 & 0 \end{pmatrix}$	$\begin{pmatrix} 0 & -1 \\ 1 & 0 \\ 0 & 0 \end{pmatrix}$	$\begin{pmatrix} 1 & 0 \\ 0 & -1 \\ 0 & 0 \end{pmatrix}$	$\begin{pmatrix} 1 & 0 \\ 0 & 0 \\ 0 & 0 \end{pmatrix}$

2 General formalism for solving the two-particle problem

We consider two spin-1/2 fermions that interact via isotropic short-range interactions. Their movement is confined to the 2D plane defined by the x and y directions. The particles' orbital motion is coupled to their spin degree of freedom via a spin-orbit coupling that depends linearly on in-plane momentum components. In addition, Zeeman spin splitting lifts the energy degeneracy of spin projections parallel to the out-of-plane (z) direction. The Hamiltonian describing such a two-particle system is given by

$$\hat{H} = \hat{H}_1^{(1)} \otimes \mathbb{1} + \mathbb{1} \otimes \hat{H}_1^{(2)} + V(\mathbf{r}_1 - \mathbf{r}_2) \quad , \quad (1)$$

where $V(\mathbf{r}_1 - \mathbf{r}_2)$ is the two-particle interaction potential, and $\hat{H}_1^{(j)}$ denotes the single-particle Hamiltonian for particle j ;

$$\hat{H}_1^{(j)} = \frac{\mathbf{p}_j^2}{2m} + h \hat{\sigma}_z + \hat{\lambda}(\mathbf{p}_j) \quad . \quad (2)$$

We use the symbol $\hat{\cdot}$ to indicate quantities that are operators in spin space, such as the vector of Pauli matrices $\hat{\sigma} \equiv (\hat{\sigma}_x, \hat{\sigma}_y, \hat{\sigma}_z)$. Spin-orbit coupling is embodied in the form of $\hat{\lambda}(\mathbf{p})$. Results obtained in this work pertain to the unitarily equivalent 2D-Dirac [42], 2D-Rashba [39–41] and 2D-Dresselhaus [7, 43] types of spin-orbit coupling, as well as the 1D type that is more straightforwardly realizable in cold-atom experiments [1]. Table 1 lists the form of $\hat{\lambda}(\mathbf{p})$ for each of these four possibilities. To enable a versatile theoretical treatment of the different spin-orbit-coupling types, we introduce a transformation for momentum vectors \mathbf{p} ,

$$\mathbf{q} \equiv (q_x, q_y, 0) = \mathcal{M} \mathbf{p} \quad , \quad (3)$$

such that $\hat{\lambda}(\mathbf{p}) = \lambda \hat{\sigma} \cdot \mathcal{M} \mathbf{p} \equiv \lambda \hat{\sigma} \cdot \mathbf{q}$. The velocity scale λ is a proportionality factor in $\hat{\lambda}(\mathbf{p})$ measuring the spin-orbit-coupling strength (see Table 1). The matrices \mathcal{M} associated with each type of spin-orbit coupling are also specified in Table 1.

The eigenstates $|\alpha_j, \mathbf{p}_j\rangle$ of the single-particle Hamiltonian (2) are labelled by the individual particle's momentum \mathbf{p}_j and a helicity quantum number $\alpha_j = \pm 1$ that distinguishes spin-split single-particle energy bands $\epsilon_{\alpha_j}(\mathbf{p}_j)$ with dispersions

$$\epsilon_{\alpha}(\mathbf{p}) = \frac{\mathbf{p}^2}{2m} + \alpha \sqrt{h^2 + \lambda^2 \mathbf{q}^2} \quad . \quad (4)$$

Using the eigenbasis of $\hat{\sigma}_z$, the single-particle eigenspinors can be written more explicitly as

$$|\alpha, \mathbf{p}\rangle = \begin{pmatrix} e^{-i\phi/2} \sqrt{\frac{Z(\mathbf{p})+\alpha b}{2Z(\mathbf{p})}} \\ \alpha e^{i\phi/2} \sqrt{\frac{Z(\mathbf{p})-\alpha b}{2Z(\mathbf{p})}} \end{pmatrix}, \quad (5)$$

with $\phi = \arg(q_x + iq_y)$. Here $Z(\mathbf{p}) = \sqrt{b^2 + \mathbf{q}^2}$ in terms of the transformed momentum \mathbf{q} [see Eq. (3)], and $b = \hbar/\lambda$ is a momentum scale set by the relative magnitudes of the Zeeman energy and the spin-orbit coupling.

To address the two-particle problem, we switch to COM and relative coordinates for the orbital motion,

$$\mathbf{R} = \frac{1}{2}(\mathbf{r}_1 + \mathbf{r}_2), \quad \mathbf{r} = \mathbf{r}_1 - \mathbf{r}_2, \quad \mathbf{P} = \mathbf{p}_1 + \mathbf{p}_2, \quad \mathbf{p} = \frac{1}{2}(\mathbf{p}_1 - \mathbf{p}_2), \quad (6)$$

and introduce the total-spin operator

$$\hat{\Sigma} = \frac{1}{2}(\hat{\sigma} \otimes \mathbb{1} + \mathbb{1} \otimes \hat{\sigma}) \quad (7)$$

whose eigenstates are the familiar singlet and triplet states $|S M\rangle$ with $S \in \{0, 1\}$ and $M = -S, -S+1, \dots, S$ denoting eigenvalues of $\hat{\Sigma}_z$. It is possible to separate off the COM kinetic energy and write the two-particle Hamiltonian (1) in the form

$$\hat{H} = \frac{\mathbf{P}^2}{4m} + \hat{H}_{\mathbf{p}} + V(\mathbf{r}), \quad (8)$$

where $\hat{H}_{\mathbf{p}}$ contains the relative-motion kinetic energy and the spin-orbit coupling terms, which still depend parametrically on the COM momentum \mathbf{P} :

$$\hat{H}_{\mathbf{p}} = \frac{\mathbf{p}^2}{m} + \lambda \mathbf{q} \cdot (\hat{\sigma} \otimes \mathbb{1} - \mathbb{1} \otimes \hat{\sigma}) + 2 \mathbf{B}_{\mathbf{p}} \cdot \hat{\Sigma}. \quad (9)$$

Here we have introduced the abbreviation $\mathbf{B}_{\mathbf{p}} = (\lambda Q_x/2, \lambda Q_y/2, \hbar)$, where $\mathbf{Q} = \mathcal{M}\mathbf{P}$ with the matrix \mathcal{M} associated with the spin-orbit-coupling type as per Table 1. Thus COM momentum affects the relative motion when spin-orbit coupling is finite via a Zeeman-like coupling to the in-plane total-spin components. Also, $[\hat{\Sigma}^2, \hat{H}_{\mathbf{p}}] \neq 0$ due to the second term in Eq. (9), indicating that two-particle eigenstates will generally be superpositions of the eigenstates $|S M\rangle$ for total spin when $\lambda \neq 0$.

We now proceed to solve the relative-motion problem embodied by the Hamiltonian $\hat{H}_{\mathbf{p}} + V(\mathbf{r})$, where the total momentum \mathbf{P} enters as a vector-valued parameter. We first consider the situation of noninteracting particles and then solve the two-particle bound-state problem.

2.1 Case of noninteracting particles

In the absence of interactions, the two-particle eigenstates are eigenstates of $\hat{H}_{\mathbf{p}}$, which can be written as antisymmetrized products of the individual particles' helicity and momentum eigenstates;

$$|\mathbf{p}; \alpha_1, \alpha_2\rangle_{\mathbf{p}} = \mathcal{A}[|\mathbf{p}\rangle |\alpha_1, \alpha_2\rangle_{\mathbf{p}, \mathbf{p}}] \equiv \frac{1}{\sqrt{2}}(|\mathbf{p}\rangle |\alpha_1, \alpha_2\rangle_{\mathbf{p}, \mathbf{p}} - |-\mathbf{p}\rangle |\alpha_2, \alpha_1\rangle_{-\mathbf{p}, \mathbf{p}}). \quad (10)$$

Here, $|\mathbf{p}\rangle$ denotes a relative-momentum eigenstate, and \mathcal{A} is the antisymmetrization operator. Throughout this paper, we use a notation where $|\cdot\rangle$ denotes states for the relative-orbital-motion degree of freedom, $|\cdot\rangle$ are spin states, and $|\cdot\rangle\rangle$ are full two-particle states in the product space of spin and orbital degrees of freedom. The two-particle spin state $|\alpha_1, \alpha_2\rangle_{\mathbf{p}, \mathbf{P}}$ is a product state of single-particle helicity states given in Eq. (5);

$$|\alpha_1, \alpha_2\rangle_{\mathbf{p}, \mathbf{P}} = |\alpha_1, \mathbf{P}/2 + \mathbf{p}\rangle \otimes |\alpha_2, \mathbf{P}/2 - \mathbf{p}\rangle \quad . \quad (11)$$

The associated two-particle eigenenergies are

$$\varepsilon_{\mathbf{P}}(\alpha_1, \alpha_2, \mathbf{p}) = \frac{\mathbf{p}^2}{m} + \alpha_1 \lambda Z_+ + \alpha_2 \lambda Z_- \quad , \quad (12)$$

with the definitions

$$Z_{\pm} = \sqrt{b^2 + \left(\frac{\mathbf{Q}}{2} \pm \mathbf{q}\right)^2} \quad . \quad (13)$$

2.2 Bound states resulting from s-wave attraction

A bound state is a solution of the Schrödinger equation

$$[\hat{H}_{\mathbf{P}} + V(\mathbf{r})] |\psi_b\rangle\rangle = E_b |\psi_b\rangle\rangle \quad (14)$$

with an energy below the lowest energy of the noninteracting case given in Eq. (12). This energy, which we will call the threshold energy E_{th} , is twice the minimum of the single-particle energy Eq. (4);

$$E_{\text{th}} = -\frac{\hbar^2}{m\lambda^2} - \frac{\mathbf{Q}^2}{4m\lambda^2} - m\lambda^2 \quad . \quad (15)$$

Thus we look for eigenstates $|\psi_b\rangle\rangle$ of $\hat{H}_{\mathbf{P}} + V(\mathbf{r})$ that satisfy $E_b < E_{\text{th}}$, with both E_b and E_{th} depending parametrically on the COM momentum \mathbf{P} . The Schrödinger equation can then be formally solved via

$$|\psi_b\rangle\rangle = \frac{1}{E_b - \hat{H}_{\mathbf{P}}} V |\psi_b\rangle\rangle \quad , \quad (16)$$

as the denominator on the right-hand side is never zero because the bound-state energy is outside the eigenvalue spectrum of $\hat{H}_{\mathbf{P}}$. We can expand the full bound-state wave function with respect to the relative-momentum eigenbasis,

$$|\psi_b\rangle\rangle = \int \frac{d^2 p'}{(2\pi\hbar)^2} (\mathbf{p}' | \psi_b\rangle\rangle) |\mathbf{p}'\rangle \quad , \quad (17)$$

keeping in mind that the expansion "coefficients" $(\mathbf{p}' | \psi_b\rangle\rangle) \equiv |\psi_b(\mathbf{p}')\rangle$ are actually still kets in spin space that parametrically depend on the total momentum \mathbf{P} . Inserting the expansion (17) on the r.h.s. of Eq. (16) and projecting both sides onto $|\mathbf{p}\rangle$, we obtain

$$|\psi_b(\mathbf{p})\rangle = \frac{1}{E_b - \hat{H}_{\mathbf{P}}} \int \frac{d^2 p'}{(2\pi\hbar)^2} (\mathbf{p} | V | \mathbf{p}') |\psi_b(\mathbf{p}')\rangle \equiv \hat{G}_{\mathbf{P}}(E_b, \mathbf{p}) \int \frac{d^2 p'}{(2\pi\hbar)^2} (\mathbf{p} | V | \mathbf{p}') |\psi_b(\mathbf{p}')\rangle \quad , \quad (18)$$

where the Green's function $\hat{G}_{\mathbf{P}}(E, \mathbf{p})$ is an operator (a 4×4 matrix) in two-particle spin space.

A general isotropic interaction potential can be expanded in partial waves, yielding

$$\langle \mathbf{p} | V | \mathbf{p}' \rangle = \sum_{l=-\infty}^{\infty} V_l(\mathbf{p}, \mathbf{p}') e^{il(\phi_{\mathbf{p}} - \phi_{\mathbf{p}'})} . \quad (19)$$

Here $\phi_{\mathbf{p}}$ is the polar angle of the vector \mathbf{p} . Furthermore, as the eigenstates $|S M\rangle$ of total spin form a basis in two-particle spin space, we can expand

$$|\psi_b(\mathbf{p})\rangle = \sum_{S,M} |S M\rangle \langle S M | \psi_b(\mathbf{p}) \rangle \quad (20)$$

where, due to the antisymmetry requirement of two-fermion wave functions, $\langle 00 | \psi_b(\mathbf{p}) \rangle$ must be an even function of \mathbf{p} , whereas the functions $\langle 1M | \psi_b(\mathbf{p}) \rangle$ must be odd. Inserting both (19) and (20) into the r.h.s. of (18) yields

$$|\psi_b(\mathbf{p})\rangle = \sum_{S,M} \hat{G}_{\mathbf{p}}(E_b, \mathbf{p}) |S M\rangle \sum_l \int \frac{d^2 p'}{(2\pi\hbar)^2} V_l(\mathbf{p}, \mathbf{p}') e^{il(\phi_{\mathbf{p}} - \phi_{\mathbf{p}'})} \langle S M | \psi_b(\mathbf{p}') \rangle . \quad (21)$$

For the case of short-range, low-energy, s -wave scattering, $V_l(\mathbf{p}, \mathbf{p}') \rightarrow V_0 \delta_{l,0}$ and the integral on the r.h.s. of Eq. (21) remains finite (vanishes) for the singlet(triplet)-state contribution(s) because the integrand is an even (odd) function of \mathbf{p}' . Thus the bound-state wave function is obtained by the action of the Green's function on the singlet state;

$$|\psi_b(\mathbf{p})\rangle = c_{\mathbf{p}} V_0 \hat{G}_{\mathbf{p}}(E_b, \mathbf{p}) |00\rangle , \quad (22)$$

with the \mathbf{P} -dependent prefactor

$$c_{\mathbf{p}} = \int \frac{d^2 p'}{(2\pi\hbar)^2} \langle 00 | \psi_b(\mathbf{p}') \rangle . \quad (23)$$

The amplitudes $\langle S M | \psi_b(\mathbf{p}) \rangle$ for the s -wave-attraction-generated bound state (22) can be neatly expressed in terms of matrix elements of the Green's function,

$$\langle S M | \psi_b(\mathbf{p}) \rangle = c_{\mathbf{p}} V_0 \langle S M | \hat{G}_{\mathbf{p}}(E_b, \mathbf{p}) |00\rangle , \quad (24)$$

for which we have obtained the general analytical expressions (see Appendix B for details of the derivation)

$$\langle 00 | \hat{G}_{\mathbf{p}}(E_b, \mathbf{p}) |00\rangle = -\frac{s}{d} (s^2 - 4h^2 - \lambda^2 \mathbf{Q}^2) \equiv -\frac{s}{d} (s^2 - 4\mathbf{B}_{\mathbf{p}}^2) , \quad (25a)$$

$$\langle 10 | \hat{G}_{\mathbf{p}}(E_b, \mathbf{p}) |00\rangle = -\frac{2\lambda}{d} [2\lambda h \mathbf{Q} \cdot \mathbf{q} - i s (\mathbf{Q} \times \mathbf{q})_z] , \quad (25b)$$

$$\langle 11 | \hat{G}_{\mathbf{p}}(E_b, \mathbf{p}) |00\rangle = -\frac{\sqrt{2}\lambda}{d} [\lambda^2 \mathbf{Q} \cdot \mathbf{q} (Q_x - i Q_y) + (s^2 + 2sh)(q_x - i q_y)] , \quad (25c)$$

$$\langle 1-1 | \hat{G}_{\mathbf{p}}(E_b, \mathbf{p}) |00\rangle = -\frac{\sqrt{2}\lambda}{d} [\lambda^2 \mathbf{Q} \cdot \mathbf{q} (Q_x + i Q_y) + (s^2 - 2sh)(q_x + i q_y)] . \quad (25d)$$

Here we used the abbreviation

$$d = s^4 - 4\lambda^2 s^2 (b^2 + \mathbf{q}^2 + \mathbf{Q}^2/4) + 4\lambda^4 (\mathbf{Q} \cdot \mathbf{q})^2 \equiv s^4 - 4s^2 (\mathbf{B}_{\mathbf{p}}^2 + \lambda^2 \mathbf{q}^2) + 16\lambda^2 (\mathbf{B}_{\mathbf{p}} \cdot \mathbf{q})^2 , \quad (26)$$

and $s = \mathbf{p}^2/m - E_b$. The expressions (24) to (26) for the bound-state wave function extend similar expressions given in Ref. [35] for the case with $\hbar = 0$ by fully accounting for nonzero Zeeman spin splitting. Based on the expansion (20) with amplitudes (24), we define the fractional weights of total-spin eigenstates in the bound-state wave function as

$$N_{SM} = \frac{\int d^2p \left| \langle SM | \hat{G}_{\mathbf{p}}(E_b, \mathbf{p}) | 00 \rangle \right|^2}{\sum_{S,M} \int d^2p \left| \langle SM | \hat{G}_{\mathbf{p}}(E_b, \mathbf{p}) | 00 \rangle \right|^2} . \quad (27)$$

2.3 Binding energy from the Bethe-Peierls boundary condition

A secular equation for the bound-state energy can be found by projecting Eq. (22) onto the singlet state and integrating over momentum, which yields

$$\frac{1}{V_0} = \int \frac{d^2p}{(2\pi\hbar)^2} \langle 00 | \hat{G}_{\mathbf{p}}(E_b, \mathbf{p}) | 00 \rangle , \quad (28)$$

with the matrix element of the Green's function between singlets given explicitly in Eq. (25a). Although principally correct, Eq. (28) turns out to be impractical for determining bound-state energies because the integral on its r.h.s. is ultraviolet-divergent. *Ad hoc* cut-offs have sometimes been introduced to circumvent this issue [35]. Here we address the problem using the Bethe-Peierls boundary condition for a scattering wave function in 2D.

We consider the equivalent of Eq. (22) in real space,

$$|\psi_b(\mathbf{r})\rangle = N \hat{g}_{\mathbf{p}}(E_b, \mathbf{r}) | 00 \rangle , \quad (29)$$

where N is a normalization factor and $g(E_b, \mathbf{r})$ denotes the real-space Green's function

$$\hat{g}_{\mathbf{p}}(E_b, \mathbf{r}) = \int \frac{d^2p}{(2\pi\hbar)^2} e^{\frac{i\mathbf{p}\cdot\mathbf{r}}{\hbar}} \hat{G}_{\mathbf{p}}(E_b, \mathbf{p}) . \quad (30)$$

Its matrix element between singlets is found as

$$\begin{aligned} \langle 00 | \hat{g}_{\mathbf{p}}(E_b, \mathbf{r}) | 00 \rangle &= \\ &= \frac{1}{(2\pi\hbar)^2} \int d^2p \sum_{\alpha_1, \alpha_2} e^{\frac{i\mathbf{p}\cdot\mathbf{r}}{\hbar}} |\langle 00 | \alpha_1, \alpha_2 \rangle_{\mathbf{p}, \mathbf{p}}|^2 \left(\frac{1}{E_b - \varepsilon_{\mathbf{p}}(\alpha_1, \alpha_2, \mathbf{p})} - \frac{1}{E_b - \mathbf{p}^2/m} \right) \\ &+ \frac{1}{(2\pi\hbar)^2} \int d^2p e^{\frac{i\mathbf{p}\cdot\mathbf{r}}{\hbar}} \frac{1}{E_b - \mathbf{p}^2/m} , \end{aligned} \quad (31)$$

where the first term on the right-hand side is regular and we have separated off the second term, which diverges logarithmically for $|\mathbf{r}| = 0$. This second term evaluates explicitly to a modified Bessel function

$$\frac{1}{(2\pi\hbar)^2} \int d^2p e^{\frac{i\mathbf{p}\cdot\mathbf{r}}{\hbar}} \frac{1}{E_b - \mathbf{p}^2/m} = -\frac{m}{2\pi\hbar^2} K_0(-i|\mathbf{r}|\sqrt{mE_b}/\hbar) , \quad (32)$$

for which the small- $|\mathbf{r}|$ behavior is known. Thus we can expand the Green's function in the short-range limit $|\mathbf{r}| \rightarrow 0$ as

$$\langle 00 | \hat{g}_{\mathbf{p}}(E_b, \mathbf{r}) | 00 \rangle \approx \frac{m}{2\pi\hbar^2} \left[\ln(|\mathbf{r}|\sqrt{-mE_b}/2\hbar) + \gamma + F_{\mathbf{p}}(E_b, \hbar) \right] , \quad (33)$$

with finite spin-orbit coupling giving rise to the \mathbf{r} -independent contribution

$$\begin{aligned}
 F_{\mathbf{P}}(E_b, h) &= \frac{1}{m} \int \frac{d^2 p}{2\pi} \sum_{\alpha_1, \alpha_2} |\langle 00 | \alpha_1, \alpha_2 \rangle_{\mathbf{P}, \mathbf{P}}|^2 \left(\frac{1}{E_b - \varepsilon_{\mathbf{P}}(\alpha_1, \alpha_2, \mathbf{P})} - \frac{1}{E_b - \mathbf{p}^2/m} \right), \\
 &= \frac{1}{m} \int \frac{d^2 p}{2\pi} \left(\langle 00 | \hat{G}_{\mathbf{P}}(E_b, \mathbf{P}) | 00 \rangle + \frac{1}{s} \right) \equiv \frac{1}{m} \int \frac{d^2 p}{2\pi} \left(\frac{16(\mathbf{B}_{\mathbf{P}} \cdot \mathbf{q})^2 - 4s^2 \lambda^2 \mathbf{q}^2}{s d} \right). \quad (34)
 \end{aligned}$$

For the singlet component of the bound-state wave function, the short-range behavior is described by Bethe-Peierls boundary conditions [44] which, for 2D systems, have a logarithmic divergence

$$\langle 00 | \psi_b(\mathbf{r}) \rangle = B \langle 00 | \hat{g}_{\mathbf{P}}(E_b, \mathbf{r}) | 00 \rangle \propto \ln(|\mathbf{r}|/a_{2D}) \quad . \quad (35)$$

Unlike their 3D counterparts, in two spatial dimensions there is no additional term added due to the spin-orbit coupling [45]. Matching the Bethe-Peierls boundary condition (35) to the short-range limit of the singlet projection for the bound-state wave function given in Eq. (33), we obtain the implicit equation

$$\gamma + \ln(a_{2D} \sqrt{-m E_b} / 2\hbar) + F_{\mathbf{P}}(E_b, h) = 0 \quad (36)$$

for the bound state energy E_b . For convenience, we parameterize the two-particle interaction strength in terms of the energy scale $\epsilon_0 = \hbar^2 / m a_{2D}^2$ and introduce dimensionless quantities $\tilde{E}_b = E_b / (m \lambda^2)$, $\tilde{h} = h / (m \lambda^2)$ and $\tilde{\epsilon}_0 = \epsilon_0 / (m \lambda^2)$. In terms of these, Eq. (36) becomes

$$\gamma + \ln \left(\frac{1}{2} \sqrt{\frac{-\tilde{E}_b}{\tilde{\epsilon}_0}} \right) = -F_{\mathbf{P}}(\tilde{E}_b, \tilde{h}) \quad . \quad (37)$$

In the absence of spin-orbit coupling, i.e., for $\lambda \rightarrow 0$, the r.h.s of Eq. (37) vanishes and $E_b \rightarrow -4 e^{-2\gamma} \epsilon_0$ is obtained, reproducing the well-known result [44] for the two-particle bound-state energy in two spatial dimensions.

3 Bound-state properties for 2D-type spin-orbit coupling

In this section, we consider the bound-state problem for the case of 2D-type spin-orbit couplings of the Dirac, Rashba or Dresselhaus forms (see Table 1). The bound state's energy and conditions for its existence are the same for all three forms, but the bound-state wave function is different for each of these.

3.1 Case of zero center-of-mass momentum

We first assume $\mathbf{P} = 0$. In this case, we can obtain an analytic expression for the quantity $F_{\mathbf{P}}(E_b, h)$ that appears on the r.h.s. of Eq (37);

$$\begin{aligned}
 F_0(\tilde{E}_b, \tilde{h}) &= -\frac{1}{4(\tilde{h}^2 + \tilde{E}_b)} \left[\frac{2(2\tilde{h}^2 + \tilde{E}_b)}{\sqrt{-1 - \tilde{h}^2 - \tilde{E}_b}} \left(\frac{\pi}{2} + \arctan \left(\frac{\tilde{E}_b + 2}{2\sqrt{-1 - \tilde{h}^2 - \tilde{E}_b}} \right) \right) \right. \\
 &\quad \left. - \tilde{E}_b (-2 \ln(-\tilde{E}_b) + \ln(\tilde{E}_b^2 - 4\tilde{h}^2)) \right]. \quad (38)
 \end{aligned}$$

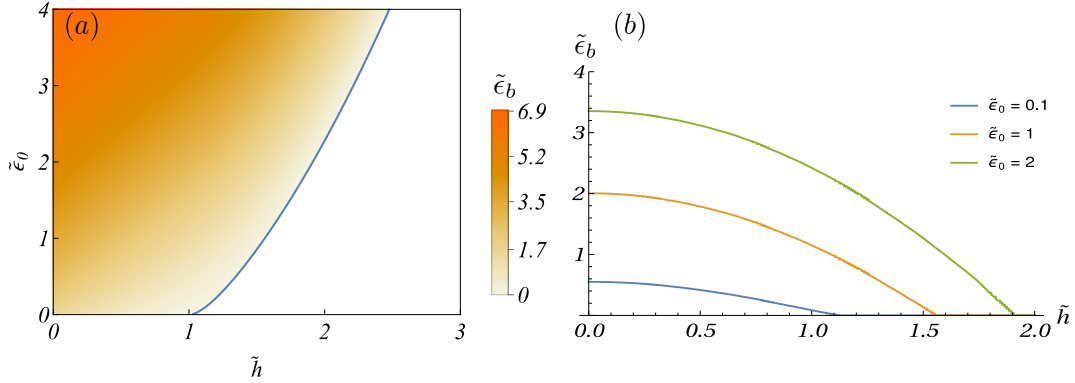


Figure 1: Binding energy of a 2D-fermion dimer with zero center-of-mass momentum ($\mathbf{P} = 0$) formed in the presence of 2D-type spin-orbit coupling and Zeeman splitting. Orange color in panel (a) indicates the parameter region where a bound state exists. The analytical result (39) for its boundary is indicated by the solid blue line. Here $\tilde{\epsilon}_0 \equiv \epsilon_0/(m\lambda^2)$ and $\tilde{h} \equiv h/(m\lambda^2)$ are the s -wave interaction strength and the Zeeman energy, respectively, measured in units of the spin-orbit-coupling energy scale $m\lambda^2$. The dimensionless binding energy $\tilde{\epsilon}_b \equiv \epsilon_b/(m\lambda^2)$ is represented by the color scale in panel (a) and plotted as a function of \tilde{h} for selected values of $\tilde{\epsilon}_0$ in panel (b).

For given dimensionless interaction strength $\tilde{\epsilon}_0$ and Zeeman energy \tilde{h} , Eq. (37) constitutes an implicit equation for the bound-state energy \tilde{E}_b , which we find to have at most one solution. Figure 1 shows plots of the dimensionless binding energy $\tilde{\epsilon}_b = \tilde{E}_{\text{th}} - \tilde{E}_b$, which is the difference between the threshold energy \tilde{E}_{th} (the lowest energy unbound fermions can have) and the bound-state energy, as a function of these parameters. For small-enough Zeeman splitting $\tilde{h} \leq 1$, a bound state always exists but, for $\tilde{h} > 1$, having a bound state requires sufficiently strong attractive interactions. The white area shown in Fig. 1(a) indicates the parameter range for which no bound state exists. The minimum dimensionless interaction strength $\tilde{\epsilon}_0^{\text{crit}}(\tilde{h})$ needed to maintain a bound state at finite Zeeman splitting can be found by substituting the threshold energy $\tilde{E}_{\text{th}} = -1 - \tilde{h}^2$ into Eq (37), which yields (see Appendix C for mathematical details)

$$\tilde{\epsilon}_0^{\text{crit}}(\tilde{h}) = e^{2\gamma+2} \frac{1 + \tilde{h}^2}{4} \left(\frac{\tilde{h}^2 - 1}{\tilde{h}^2 + 1} \right)^{1+\tilde{h}^2} \Theta(\tilde{h} - 1) . \quad (39)$$

Here $\Theta(\cdot)$ denotes the Heaviside step function. We show $\tilde{\epsilon}_0^{\text{crit}}(\tilde{h})$ as the blue solid line in Fig. 1(a). As is apparent from Fig. 1(b), the binding energy approaches zero continuously at this boundary.

It is known that the combination of s -wave attraction and spin-orbit coupling can result in behavior analogous to a system subject to p -wave interactions without spin-orbit coupling [22]. In our case, this would manifest as having also triplet components of the bound-state wave function, even though the attractive potential is s -wave. In the case without spin-orbit coupling, s -wave interactions at low energy only lead to binding in the singlet channel, and the overlap of the wave function to the triplet component would vanish, as the Green's function in Eq. (22) would be diagonal in spin space. However, although the s -wave interaction potential projects the wave function onto the singlet, the subsequent free propagation in the presence of spin-orbit coupling rotates parts of the wave function back into the triplet channel. In particular, we are interested to understand in which regime a large triplet component of the bound state develops. Naively, we

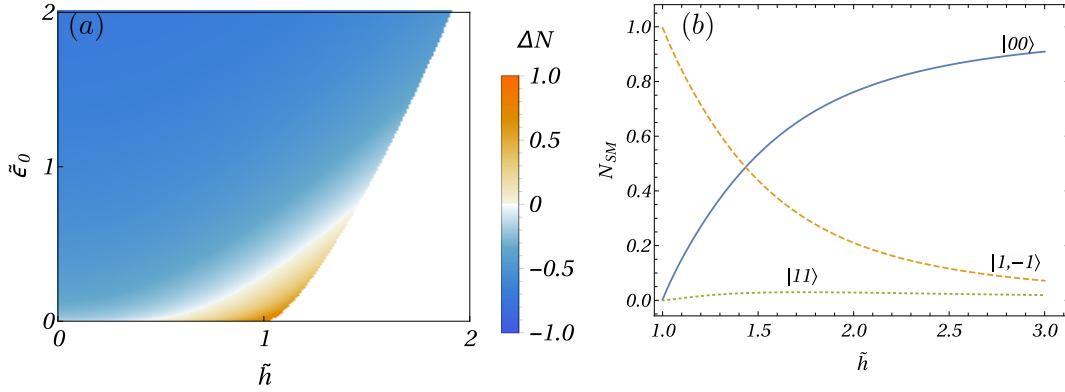


Figure 2: Triplet-state admixture to 2D-fermion bound states with zero center-of-mass momentum. The color scale in panel (a) visualizes the difference $\Delta N = \sum_M N_{1M} - N_{00}$ between the combined fractional weights of triplet states contributing to the dimer and that of the singlet-state contribution. Panel (b) shows plots of N_{SM} (except for $N_{10} = 0$) for total-spin eigenstates in bound states formed for parameter combinations $(\tilde{h}, \tilde{\epsilon}_0) \equiv (\tilde{h}^{\text{crit}}, \tilde{\epsilon}_0^{\text{crit}})$ corresponding to the blue line shown in Fig. 1(a), with $\tilde{\epsilon}_0^{\text{crit}} [\tilde{h}^{\text{crit}}]$ given by Eq. (39) [by inverting Eq. (39)].

may expect that, for large Zeeman splitting, the triplet state $|1 - 1\rangle$ would dominate the system as it is energetically favored. The same behavior is also seen in the BCS mean-field theory of the many-body system where the topological superfluid with p -wave order parameter emerges for large Zeeman splitting [21,22,26]. However, as we see below, only a relatively small region around the critical magnetic field $h = m\lambda^2$ for weak attractive interaction exists where the bound-state wave function is dominated by the triplet components.

We obtain the fractional weights of total-spin eigenstates contributing to the bound-state wave function via Eq. (27), utilizing the expressions (25) for Green's-function matrix elements. In the limit of vanishing COM momentum, we obtain analytical formulae (see Appendix D), which are however very long and not illuminating — except for the triplet state $|10\rangle$ that makes no contribution to the bound state when $\mathbf{P} = 0$. Figure 2(a) shows the difference $\Delta N \equiv \sum_M N_{1M} - N_{00}$ between the combined fractional weights for triplet states and that of the singlet state for part of the parameter space depicted in Fig. 1(a). The quantity ΔN constitutes a measure for the triplet character of the two-particle bound state as, by construction, $-1 \leq \Delta N \leq 1$, where $\Delta N = 1$ indicates a pure triplet and $\Delta N = -1$ a pure singlet state. From Fig. 2(a), we see that the triplet contribution to the bound state dwarfs the singlet part in a region around $\tilde{h} = 1$ and sufficiently weak interaction strength $\tilde{\epsilon}_0 \lesssim 1$, suggesting that p -wave character of the bound-state wave function should be prevalent there. The values N_{SM} for individual triplet states are plotted in Fig. 2(b) for the parameter pairs $(\tilde{h}^{\text{crit}}, \tilde{\epsilon}_0^{\text{crit}})$ along the boundary of the region of existence for bound states in Fig. 1(a), given explicitly by Eq. (39). Asymptotically, as $\tilde{\epsilon}_0 \rightarrow 0$ and $\tilde{h} \rightarrow 1$, the bound-state wave function becomes the state $|1 - 1\rangle$.

3.2 Effect of finite center-of-mass momentum

For nonzero COM momentum, we can repeat the steps described in the previous section. While we were not able to find closed-form analytic expressions for the quantity appearing on the r.h.s. of Eq. (37), numerical solutions for the bound state energy and the fractional weights of the total-spin

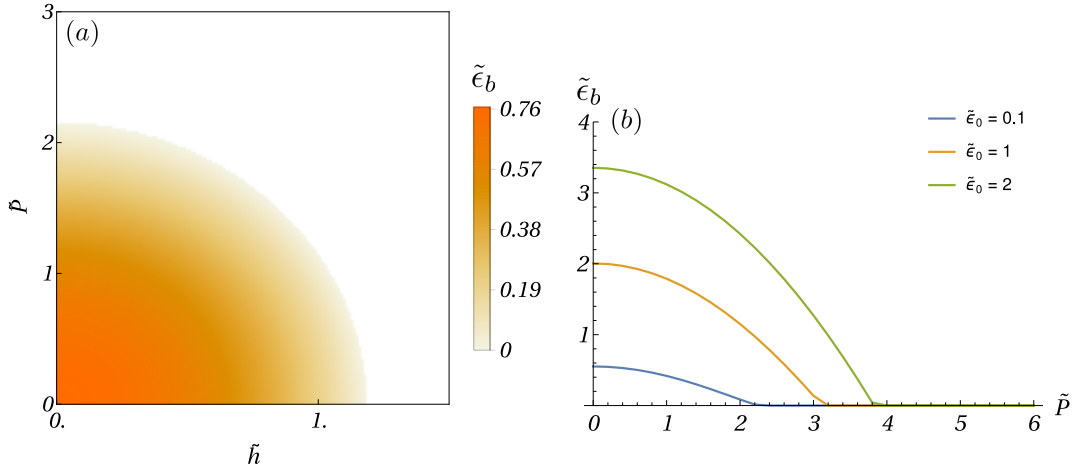


Figure 3: Effect of finite center-of-mass momentum \mathbf{P} on dimer formation. Orange color in panel (a) indicates the range for dimensionless parameters quantifying the COM-momentum magnitude [$\tilde{P} \equiv |\mathbf{P}|/(m\lambda)$] and the Zeeman energy [$\tilde{h} \equiv h/(m\lambda^2)$] within which a 2D-fermion bound state exists. The color scale represents the dimensionless binding energy $\tilde{\epsilon}_b \equiv \epsilon_b/(m\lambda^2)$. Data shown in panel (a) are obtained for a fixed value $\tilde{\epsilon}_0 = 0.2$ of the dimensionless interaction strength. Panel (b) shows plots of $\tilde{\epsilon}_b$ as a function of \tilde{P} for selected other values of $\tilde{\epsilon}_0$ and fixed $\tilde{h} = 0$.

eigenstates (27) can be readily obtained. In Fig. 3(a), we plot the binding energy at weak interactions ($\tilde{\epsilon}_0 = 0.2$) for finite Zeeman splitting and COM momenta. We see that, as we discussed earlier in this paper, COM momentum acts just like an effective Zeeman coupling. Specifically, as we plot the binding energy in the plane spanned by the variables \tilde{h} and $\tilde{P}/2$, the region where the bound state exists exhibits a circular symmetry. In Fig. 3(b), we plot the binding energy at zero Zeeman energy as a function of COM momentum and observe a similar dependence on the COM momentum as seen in Fig. 1(b) as function of the Zeeman spin splitting. The weakening and eventual loss of the bound state with finite COM momentum is a well known property of dimers in the presence of spin-orbit coupling [29, 35]. It implies that, e.g., in a not fully condensed gas with a momentum distribution of a certain width, bound pairs at the outer edge of this distribution are no longer bound; thus such a setup would contain both bound pairs and unbound atoms. In a time-of-flight measurement, the unbound atoms are expected to form a ring around the bound pairs closer to the center of the momentum distribution [29].

As Fig. 3(a) shows, Zeeman splitting and (the suitably rescaled) COM momentum are equivalent in their effect on the bound-state formation and its energy. However, details of the bound-state structure are different in the two cases. To illustrate this, we consider the fractional weights of total-spin eigenstates in the bound-state wave function, evaluating the integrals entering the expressions (27) numerically. In Fig. 4(a), we plot the difference ΔN between the combined weights of all triplet states and that of the singlet state as a function of \tilde{h} and \tilde{P} for fixed $\tilde{\epsilon}_0 = 0.2$. While triplet character always dominates along the outer boundary of the parameter region where dimers are formed, the pattern does not fully exhibit the rotational symmetry seen in Fig. 3(a). Furthermore, in Fig. 4(b), we plot the individual fractional weights of total-spin eigenstates making up the bound state for $\tilde{h} = 0$. Here we see that, for finite COM momenta close to the boundary of the bound state region, the triplet state $|10\rangle$ has the largest weight, whereas this state does not contribute at all to the zero-COM-momentum bound state (see Sec. 3.1). Thus the type of domi-

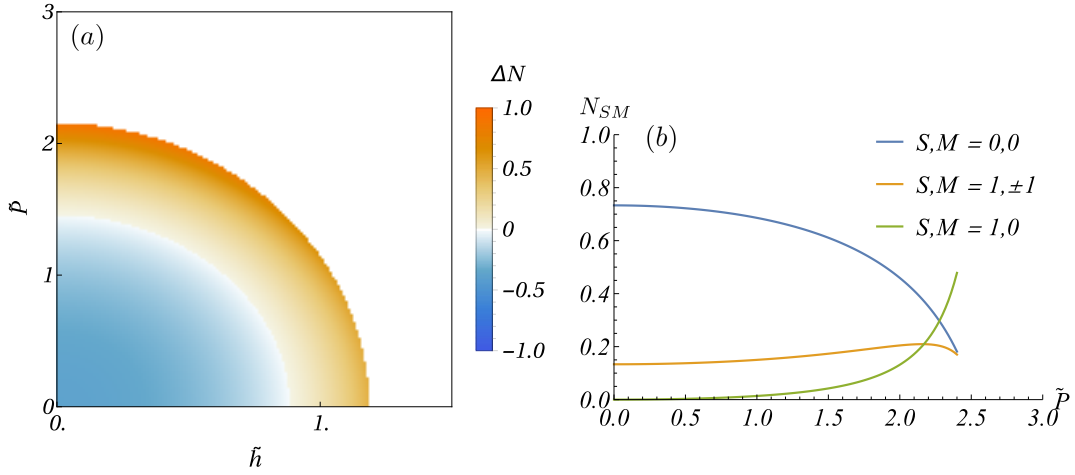


Figure 4: Bound-state triplet admixture for dimers with finite center-of-mass momentum. Panel (a) shows the quantity $\Delta N = \sum_M N_{1M} - N_{00}$, which measures the balance between triplet and singlet character in the 2D-fermion dimer, as a function of the same set of parameters as in Fig. 3(a). The relative weights of individual total-spin eigenstates contributing to the bound-state wave function are plotted in panel (b) as a function of \tilde{P} for fixed $\tilde{h} = 0$, which is the parameter range along the vertical axis in panel (a).

nating triplet character differs crucially depending on how it is generated: large Zeeman splitting renders a spin-polarized triplet state to be dominant, whereas large COM momentum favors the spin-unpolarized triplet state.

4 Bound states formed with 1D-type spin-orbit coupling

The 1D-type spin-orbit coupling $\hat{\lambda}(\mathbf{p}) = \lambda p_x \hat{\sigma}_x$ is not isotropic since a particular in-plane direction is singled out. As a consequence, the COM-dependent contribution to the Zeeman coupling has only an x component, $\mathbf{B}_{\mathbf{p}} = (\lambda P_x/2, 0, h)$, i.e., only one component of the COM momentum affects the bound-state properties.

Specializing the general formulae from Sec. 2 to the case with 1D-type spin-orbit coupling means adopting $\mathbf{B}_{\mathbf{p}} = (\lambda P_x/2, 0, h)$, $\mathbf{Q} = (P_x, 0, 0)$ and $\mathbf{q} = (q_x, 0, 0)$. The resulting form of the implicit equation (37) for the bound-state energy can only be solved numerically. For the case of zero COM momentum ($P_x = 0$), we calculate the binding energy for the same range of Zeeman-energy values and s -wave-interaction strengths as in the previous section. Results are shown in Fig. 5(a). We find that the parameter region within which a bound state exists is larger than in the case of 2D-type spin-orbit coupling. To illustrate this, the boundary line that we derived in Eq. (39) for the 2D-type case is drawn as the dashed curve for comparison. In addition, the binding energy is generally higher than with 2D-type spin-orbit coupling.

We also adapt the formalism presented in Sec. 2.2 for calculating the fractional weights N_{SM} of total-spin eigenstates in the bound state to the case of 1D-type spin-orbit coupling. This amounts to using $\mathbf{B}_{\mathbf{p}} = (\lambda P_x/2, 0, h)$, $\mathbf{Q} = (P_x, 0, 0)$ and $\mathbf{q} = (p_x, 0, 0)$ in Eqs. (25). In Fig. 5(b), the difference ΔN between total weight from triplet states contributing to the bound state and the weight of the singlet state are shown. The results are different from the case with 2D-type spin-

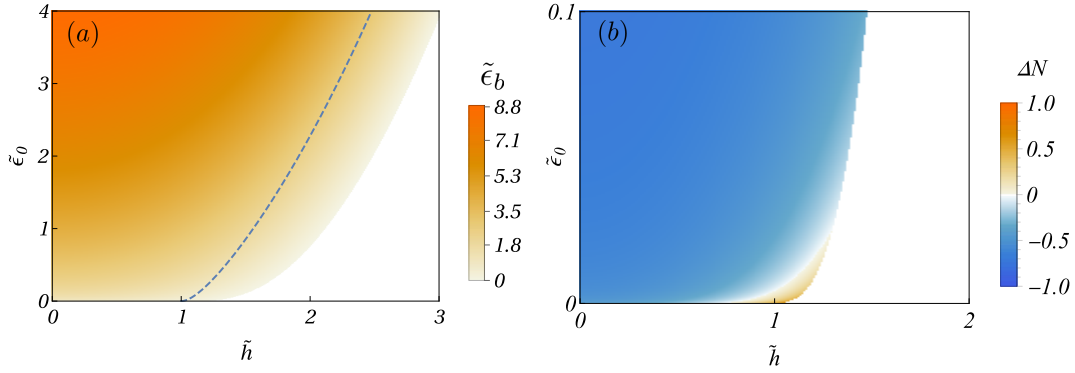


Figure 5: Dimensionless binding energy $\tilde{\epsilon}_b$ [panel (a)] and bound-state triplet character quantified by $\Delta N \equiv \sum_M N_{1M} - N_{00}$ [panel (b)] of 2D-fermion dimers with zero center-of-mass momentum formed in the presence of 1D-type spin-orbit coupling and Zeeman splitting. These plots can be compared with corresponding results for the 2D-type spin-orbit couplings shown in Figs. 1(a) and 2(a), respectively. The dashed blue line in panel (a) is the critical line delimiting bound-state existence in Fig. 1(a). Evidently, the existence region for bound states formed with asymmetric spin-orbit coupling extends well beyond.

orbit coupling, as we see that binding mostly occurs in the singlet channel. However, there still is a parameter region around $\tilde{h} = 1$ at quite weak interactions where the dimer exhibits dominantly triplet character. Figure 6 shows a comparison in the interaction-strength dependence of relative weights for the total-spin eigenstates present in bound states for 2D-type and 1D-type spin-orbit couplings. Qualitatively similar behavior is exhibited in both cases, except that the region of dominant triplet character occurs at much weaker interaction strengths in the presence of 1D-type spin-orbit coupling. This is important for experiments, as 1D-type spin-orbit coupling is easier to realize, but tuning the interactions to a sufficiently weak strength (e.g. near the zero-crossing of a Feshbach resonance) might prove challenging.

5 Orbital characteristics of the bound-state wave function

In previous sections, we have discussed the binding energy and the spin properties of two-particle bound states. We now explore features in the orbital part of the bound-state wave function. Specifically, we focus on the amplitudes $\langle S M | \psi_b(\mathbf{p}) \rangle$ appearing in its expansion (20) in terms of total-spin eigenstates.

We plot representative examples obtained for 2D-Dirac spin-orbit coupling in Fig. 7. It is possible to transform these results into those applicable to other 2D-type spin-orbit couplings by swapping and/or mirroring the relative-momentum axes according to the structure of \mathcal{M} -matrices given in Table 1. The singlet component, shown in panels (a) and (b), has no imaginary part and exhibits radial symmetry in the relative-momentum (\mathbf{p}) plane for vanishing COM momentum [panel (a)]. A local minimum occurs at $\mathbf{p} = 0$ as a result of spin-orbit coupling modifying the noninteracting dispersion (12), creating an energy minimum at nonzero momentum. This local minimum in the orbital wave function associated with the singlet component at vanishing COM momentum disappears for sufficiently strong interactions $\tilde{\epsilon}_0 \geq 1$. For finite COM momentum \mathbf{P}

[the case $\mathbf{P} \equiv (P, 0)$ is shown in panel (b)], the radial symmetry is broken as the singlet-wave-function amplitude gets suppressed along the direction of \mathbf{P} .

Panels (c) and (d) in Fig. 7 show the orbital part of the spin-polarized triplet state with $M = -1$ for the same set of parameters used in panels (a) and (b), respectively. This wave function is complex and, for $\mathbf{P} = \mathbf{0}$, shows typical p -wave behavior: a radially symmetric amplitude and single phase winding around the node at the origin $\mathbf{p} = \mathbf{0}$. For finite COM momentum, the phase still behaves the same, but the radial symmetry of the wave-function amplitude is broken in an analogous fashion as seen for the singlet component in panel (b). Panels (e) and (f) depict the orbital wave function for the spin-unpolarized triplet component ($S = 1, M = 0$) that is only ever finite for nonvanishing COM momentum. Without Zeeman splitting [panel (e)], this wave function is purely imaginary and proportional to the relative-momentum component perpendicular to the COM momentum [see the cross-product term in Eq. (25b)]. When the Zeeman energy is finite as well [panel (f)], the sign change in the imaginary part of the wave function turns into a full 2π phase rotation, while the node along the direction parallel to \mathbf{P} softens into a finite local minimum.

Results shown in Fig. 8 for 1D-type spin-orbit coupling look like anisotropic versions of the behavior seen for 2D-Dirac spin-orbit coupling. As the amplitudes $\langle S M | \psi_b(\mathbf{p}) \rangle$ are all real-valued in this case, there is no phase winding but simply a sign inversion in the triplet component. Instead of a radially symmetric minimum, the singlet part exhibits a saddle point at $\mathbf{p} = \mathbf{0}$.

6 Experimental detection

Bound states could be probed with radio-frequency spectroscopy [20], or with high spectral resolution using magneto-association spectroscopy [46]. Spin-selective imaging can provide information on the spin content of ultra-cold atomic gases [47]. In order to determine the relative weight of different total-spin contributions to bound states, we propose to turn off the spin-orbit-coupling fields, which projects the cold-atom population to spin eigenstates, before using spin-selective imaging of single-particle populations. The p -wave character of the bound-state wave function can be detected by time-of-flight imaging of the single-particle momentum distribution. The characteristic signature of the p -wave character of the bound state is a vortex-like momentum distribution with a hole in the center, see Fig. 7. In the regime where triplet character dominates in the bound state, a density maximum is expected at the momentum scale $m \lambda \sqrt{\tilde{\epsilon}_b + \tilde{\hbar}^2 - 1}$. A requirement for this to work is to restrict the COM momentum to values smaller than this momentum scale, which can be achieved at low-enough temperatures. The parameter regime with a large triplet component in the bound state could be probed by a fluorescence-imaging approach with single-atom spin and momentum resolution, as recently demonstrated [48]. The ratio of pairs with same and opposite spin would give a clear indication on the number of singlet or triplet pairs in the system.

7 Conclusions and outlook

In this paper, we have investigated the properties of bound states of two fermions in a 2D gas with Zeeman spin splitting and spin-orbit coupling. While spin-orbit coupling enhances binding, both the Zeeman splitting and a finite COM momentum of the dimer counteract the formation of bound states. We show that the COM momentum acts like an additional in-plane component of the Zeeman coupling. The bound state ceases to exist when either or both the Zeeman energy and

the COM momentum exceed a threshold. For 1D-type spin-orbit coupling, the binding is stronger and the Zeeman energy for which a bound state can exist is larger than for 2D-type spin-orbit coupling.

Further, we have calculated the fractional weights of individual total-spin components in the bound state. In the systems we consider in this paper, there is a competition between the s -wave interactions, which project the two-body wave function onto the singlet state, and the spin-orbit coupling, which rotates the total-spin state into the triplet sector. By this mechanism, the triplet character of the wave function can become dominant. This happens when the attractive interactions are weak and the Zeeman energy is near the critical value for the existence of a bound state. In this regime, the wave function is mostly in the triplet state that minimizes the total Zeeman energy and has a p -wave-like shape with a node at zero relative momentum. We find that, for 1D-type spin-orbit coupling, this regime where triplet states dominate occurs in a reduced parameter range as compared to systems with 2D-type spin-orbit coupling and requires very weak interactions. Nevertheless, large triplet-state fractions are still reached also for the bound states formed in the presence of 1D-type spin-orbit coupling.

With finite COM momenta, we find that the bound state also reaches dominant triplet character but now in the unpolarized $S = 1, M = 0$ triplet state. This triplet component is only present for nonzero COM momentum. These findings show that, in a many-body system such as a thermal Fermi gas, the distribution of COM momenta will lead to a gas with bound pairs in the singlet state at the center of the momentum distribution, triplet pairs further out, and unbound fermions at even higher momenta. We also discuss how such bound states could be detected experimentally; in particular, the detection of opposite-spin and same-spin correlations can reveal whether a 2D Fermi gas with spin-orbit coupling contains singlet or triplet bound pairs.

Acknowledgements

We thank Chris Vale and Paul Dyke for helpful discussions.

Funding information This work was partially supported by the [Marsden Fund](#) of New Zealand (contract nos. VUW1713 and MAU2007) from government funding managed by the Royal Society Te Apārangi.

A Singlet- and triplet-state projections of helicity product states

This section provides useful identities involving the two-particle states (11) that are direct products of single-particle energy eigenstates labelled by the individual particles' momentum \mathbf{p}_j and helicity α_j . Indicating the spin-up (spin-down) eigenstate of $\hat{\sigma}_z$ by $|\uparrow\rangle$ ($|\downarrow\rangle$), we get for the singlet projection of such states

$$\begin{aligned} \langle 00|\alpha_1, \alpha_2\rangle_{\mathbf{p}, \mathbf{p}} &= \frac{1}{\sqrt{2}} (\langle \uparrow|\alpha_1, \mathbf{p}_1\rangle \langle \downarrow|\alpha_2, \mathbf{p}_2\rangle - \langle \downarrow|\alpha_1, \mathbf{p}_1\rangle \langle \uparrow|\alpha_2, \mathbf{p}_2\rangle) \\ &= \frac{1}{\sqrt{2}} \left(\alpha_2 e^{-\frac{i}{2}(\phi_1 - \phi_2)} \sqrt{\frac{Z_+ + \alpha_1 b}{2Z_+}} \sqrt{\frac{Z_- - \alpha_2 b}{2Z_-}} - \alpha_1 e^{\frac{i}{2}(\phi_1 - \phi_2)} \sqrt{\frac{Z_+ - \alpha_1 b}{2Z_+}} \sqrt{\frac{Z_- + \alpha_2 b}{2Z_-}} \right). \end{aligned} \quad (40)$$

Analogously, for the overlap with the $S = 1, M = 0$ triplet state, we find

$$\begin{aligned} \langle 10|\alpha_1, \alpha_2\rangle_{\mathbf{p}, \mathbf{p}} &= \frac{1}{\sqrt{2}} (\langle \uparrow|\alpha_1, \mathbf{p}_1\rangle \langle \downarrow|\alpha_2, \mathbf{p}_2\rangle + \langle \downarrow|\alpha_1, \mathbf{p}_1\rangle \langle \uparrow|\alpha_2, \mathbf{p}_2\rangle) \\ &= \frac{1}{\sqrt{2}} \left(\alpha_2 e^{-\frac{i}{2}(\phi_1 - \phi_2)} \sqrt{\frac{Z_+ + \alpha_1 b}{2Z_+}} \sqrt{\frac{Z_- - \alpha_2 b}{2Z_-}} + \alpha_1 e^{\frac{i}{2}(\phi_1 - \phi_2)} \sqrt{\frac{Z_+ - \alpha_1 b}{2Z_+}} \sqrt{\frac{Z_- + \alpha_2 b}{2Z_-}} \right). \end{aligned} \quad (41)$$

For the projections onto the spin-polarized triplet states, straightforward calculation yields

$$\langle 11|\alpha_1, \alpha_2\rangle_{\mathbf{p}, \mathbf{p}} = \langle \uparrow|\alpha_1, \mathbf{p}_1\rangle \langle \uparrow|\alpha_2, \mathbf{p}_2\rangle = e^{-\frac{i}{2}(\phi_1 + \phi_2)} \sqrt{\frac{Z_+ + \alpha_1 b}{2Z_+}} \sqrt{\frac{Z_- + \alpha_2 b}{2Z_-}} \quad (42)$$

and

$$\langle 1-1|\alpha_1, \alpha_2\rangle_{\mathbf{p}, \mathbf{p}} = \langle \downarrow|\alpha_1, \mathbf{p}_1\rangle \langle \downarrow|\alpha_2, \mathbf{p}_2\rangle = e^{\frac{i}{2}(\phi_1 + \phi_2)} \sqrt{\frac{Z_+ - \alpha_1 b}{2Z_+}} \sqrt{\frac{Z_- - \alpha_2 b}{2Z_-}}. \quad (43)$$

The phases appearing in these identities are $\phi_j = \arg(p_{j,x} + i p_{j,y})$.

Relevant for calculations leading to results presented in this paper are the absolute square of the singlet projection and the latter's products with the triplet projections. To obtain more compact expressions, 3D vectors $\mathbf{Z}_\pm = (\mathbf{Q}/2 \pm \mathbf{q}, b)$ are introduced, in terms of which we find

$$|\langle 00|\alpha_1, \alpha_2\rangle_{\mathbf{p}, \mathbf{p}}|^2 = \frac{1}{4} \left(1 - \alpha_1 \alpha_2 \frac{\mathbf{Z}_+ \cdot \mathbf{Z}_-}{Z_+ Z_-} \right), \quad (44)$$

$$\langle 10|\alpha_1, \alpha_2\rangle_{\mathbf{p}, \mathbf{p}} \langle \mathbf{p}, \mathbf{p}|\alpha_1, \alpha_2|00\rangle = \frac{1}{4} \left(\frac{b(\alpha_1 Z_- - \alpha_2 Z_+)}{Z_+ Z_-} + i \alpha_1 \alpha_2 \frac{(\mathbf{Z}_+ \times \mathbf{Z}_-)_z}{Z_+ Z_-} \right), \quad (45)$$

$$\begin{aligned} \langle 11|\alpha_1, \alpha_2\rangle_{\mathbf{p}, \mathbf{p}} \langle \mathbf{p}, \mathbf{p}|\alpha_1, \alpha_2|00\rangle &= \frac{1}{4\sqrt{2}} \left(\alpha_2 e^{-i\phi_2} \frac{|\mathbf{p}_2| \sqrt{(Z_+ + \alpha_1 b)^2}}{Z_+ Z_-} \right. \\ &\quad \left. - \alpha_1 e^{-i\phi_1} \frac{|\mathbf{p}_1| \sqrt{(Z_- + \alpha_2 b)^2}}{Z_+ Z_-} \right), \end{aligned} \quad (46)$$

$$\begin{aligned} \langle 1-1|\alpha_1, \alpha_2\rangle_{\mathbf{p}, \mathbf{p}} \langle \mathbf{p}, \mathbf{p}|\alpha_1, \alpha_2|00\rangle &= \frac{1}{4\sqrt{2}} \left(\alpha_2 e^{i\phi_1} \frac{|\mathbf{p}_1| \sqrt{(Z_- - \alpha_1 b)^2}}{Z_+ Z_-} \right. \\ &\quad \left. - \alpha_1 e^{i\phi_2} \frac{|\mathbf{p}_2| \sqrt{(Z_+ - \alpha_2 b)^2}}{Z_+ Z_-} \right). \end{aligned} \quad (47)$$

B Momentum representation of the Green's function

Here, we show how to obtain somewhat compact expressions for the momentum representation of the Green's function. As we consider only s -wave interactions that couple exclusively to the singlet channel, relevant formulae always contain the Green's function acting on the singlet total-spin eigenstate to the right. Thus we need to calculate the four matrix elements

$$\langle S M|\hat{G}_{\mathbf{p}}(E, \mathbf{p})|00\rangle = \sum_{\alpha_1, \alpha_2} \frac{\langle S M|\alpha_1, \alpha_2\rangle_{\mathbf{p}, \mathbf{p}} \langle \mathbf{p}, \mathbf{p}|\alpha_1, \alpha_2|00\rangle}{E - \varepsilon_{\mathbf{p}}(\alpha_1, \alpha_2, \mathbf{p})}, \quad (48)$$

where we employed the Lehmann representation in terms of the eigenstates (10) of $\hat{H}_{\mathbf{p}}$.

Numerators appearing in (48) have been obtained in the previous section. As was first shown in Ref. [35], introducing the variable $s = p^2/m - E$ allows us to perform the sum over the four combinations of $\{\alpha_1 = \pm, \alpha_2 = \pm\}$ and obtain a more compact form of the Green's function. For illustration, we show this in detail for the singlet component:

$$\begin{aligned}
 \langle 00 | \hat{G}_{\mathbf{P}}(E, \mathbf{p}) | 00 \rangle &= \sum_{\alpha_1 \alpha_2} \frac{|\langle 00 | \alpha_1, \alpha_2 \rangle_{\mathbf{p}, \mathbf{P}}|^2}{-\lambda(\alpha_1 Z_+ + \alpha_2 Z_-) - s} \quad (49) \\
 &= \frac{1}{4} \left[\left(1 - \frac{\mathbf{Z}_+ \cdot \mathbf{Z}_-}{Z_+ Z_-} \right) \left(\frac{1}{\lambda Z_+ + \lambda Z_- - s} + \frac{1}{-\lambda Z_+ - \lambda Z_- - s} \right) \right. \\
 &\quad \left. + \left(1 + \frac{\mathbf{Z}_+ \cdot \mathbf{Z}_-}{Z_+ Z_-} \right) \left(\frac{1}{\lambda Z_+ - \lambda Z_- - s} + \frac{1}{-\lambda Z_+ + \lambda Z_- - s} \right) \right] \\
 &= -\frac{s}{2} \left[\frac{1}{s^2 - \lambda^2(Z_+ + Z_-)^2} + \frac{1}{s^2 - \lambda^2(Z_+ - Z_-)^2} \right. \\
 &\quad \left. + \frac{\mathbf{Z}_+ \cdot \mathbf{Z}_-}{Z_+ Z_-} \left(\frac{1}{s^2 - \lambda^2(Z_+ - Z_-)^2} - \frac{1}{s^2 - \lambda^2(Z_+ + Z_-)^2} \right) \right] \\
 &= -\frac{s}{d} [s^2 - \lambda^2(Z_+^2 + Z_-^2 - 2\mathbf{Z}_+ \cdot \mathbf{Z}_-)] \\
 &= -\frac{s}{d} [s^2 - \lambda^2(4b^2 + q_1^2 + q_2^2 + 2\mathbf{q}_1 \cdot \mathbf{q}_2)] \\
 &= -\frac{s}{d} [s^2 - 4\lambda^2 b^2 - \lambda^2(\mathbf{q}_1 + \mathbf{q}_2)^2] = -\frac{s}{d} [s^2 - 4\lambda^2 b^2 - \lambda^2 \mathbf{Q}^2], \quad (50)
 \end{aligned}$$

thus obtaining (25a) with (26) giving the explicit expression for the denominator d . Along the same lines, the expressions (25b), (25c) and (25d) for Green's-function matrix elements involving the triplet states are derived. Our results agree with the expressions given in Ref. [35] in the vanishing-Zeeman-splitting limit $b \rightarrow 0$.

C Boundary of parameter region where a $\mathbf{P} = \mathbf{0}$ bound state exists

For zero COM momentum, the boundary between the parameter regions with and without a bound state can be obtained analytically, by substituting the threshold energy $\tilde{E}_{\text{th}} = -1 - \tilde{h}^2$ in place of \tilde{E}_b into Eq. (37) and using the analytical expression (38) for the function appearing on the right-hand side. In the following, we assume $\tilde{h} \geq 1$ since there is always a bound state when $\tilde{h} < 1$. First we obtain

$$\begin{aligned}
 F_0(-1 - \tilde{h}^2, \tilde{h}) &= \\
 &\frac{1}{4} \left\{ 2(\tilde{h}^2 - 1) \underbrace{\lim_{\tilde{\epsilon}_b \rightarrow 0} \frac{1}{\sqrt{\tilde{\epsilon}_b}} \left[\frac{\pi}{2} + \arctan \left(\frac{1 - \tilde{h}^2}{2\sqrt{\tilde{\epsilon}_b}} \right) \right]}_{\frac{2}{\tilde{h}^2 - 1}} - (1 + \tilde{h}^2) [2 \ln(1 + \tilde{h}^2) - \ln(1 - \tilde{h}^2)^2] \right\} \\
 &= 1 - \frac{1 + \tilde{h}^2}{2} [\ln(1 + \tilde{h}^2) - \ln|\tilde{h}^2 - 1|] \quad . \quad (51)
 \end{aligned}$$

With this (using also $|\tilde{h}^2 - 1| \equiv \tilde{h}^2 - 1$ with our assumptions), Eq. (37) becomes

$$\gamma + \ln \left(\frac{1}{2} \sqrt{\frac{1 + \tilde{h}^2}{\tilde{\epsilon}_0}} \right) = -1 - \frac{1 + \tilde{h}^2}{2} \ln \left(\frac{\tilde{h}^2 - 1}{\tilde{h}^2 + 1} \right), \quad (52)$$

which can be straightforwardly solved for $\tilde{\epsilon}_0$ to yield Eq. (39).

D Fractional weight of total-spin eigenstates in $\mathbf{P} = \mathbf{0}$ bound states

To calculate the fractional weights N_{SM} of total-spin eigenstates in the two-particle bound states according to Eq. (27), integrals over the squared magnitude of Green's-function matrix elements are needed. For the case of vanishing COM momentum, we can provide analytical results for the latter:

$$\int d^2p |\langle 00 | \hat{G}_0(E_b, \mathbf{p}) | 00 \rangle|^2 = \frac{\tilde{\hbar}^2(\tilde{E}_b - 2) + \tilde{E}_b^2}{2(\tilde{\hbar}^2 + \tilde{E}_b)^2 \tilde{\epsilon}_b} - \frac{\tilde{\hbar}^4 (\ln(\tilde{E}_b^2 - 4\tilde{\hbar}^2) - 2\ln(-\tilde{E}_b))}{(\tilde{\hbar}^2 + \tilde{E}_b)^3} - \frac{\tilde{\hbar}^4}{\tilde{E}_b (\tilde{\hbar}^2 + \tilde{E}_b)^2} - \frac{(6\tilde{\hbar}^2\tilde{E}_b^3 + 4\tilde{\hbar}^6(\tilde{E}_b - 3) + \tilde{\hbar}^4(3\tilde{E}_b(3\tilde{E}_b - 4) - 8) + \tilde{E}_b^4) \left(\arctan\left(\frac{\tilde{E}_b+2}{2\sqrt{\tilde{\epsilon}_b}}\right) + \frac{\pi}{2} \right)}{4\tilde{\epsilon}_b^{3/2} (\tilde{\hbar}^2 + \tilde{E}_b)^3} \quad (53)$$

and

$$\int d^2p |\langle 1 \pm 1 | \hat{G}_0(E_b, \mathbf{p}) | 00 \rangle|^2 = \frac{2((\tilde{\hbar} \mp 1)\tilde{\hbar} + 1)\tilde{\hbar}^2 + (3\tilde{\hbar} \mp 2)\tilde{\hbar}\tilde{E}_b + \tilde{E}_b^2}{4(\tilde{\hbar}^2 + \tilde{E}_b)^2 \tilde{\epsilon}_b} - \frac{\tilde{\hbar}^2}{2(\tilde{\hbar}^2 + \tilde{E}_b)^2} + (\pm 4\tilde{\hbar}^7 + \tilde{\hbar}^4(9\tilde{E}_b^2 + 6\tilde{E}_b - 4) + 4\tilde{\hbar}^6(\tilde{E}_b - 1) \pm 6\tilde{\hbar}^5\tilde{E}_b \mp 4\tilde{\hbar}^3\tilde{E}_b + 2\tilde{\hbar}^2\tilde{E}_b(3\tilde{E}_b(\tilde{E}_b + 2) + 2) \mp 2\tilde{\hbar}\tilde{E}_b^2(\tilde{E}_b + 2) + \tilde{E}_b^3(\tilde{E}_b + 2)) \frac{\arctan\left(\frac{\tilde{E}_b+2}{2\sqrt{\tilde{\epsilon}_b}}\right) + \frac{\pi}{2}}{8\tilde{\epsilon}_b^{3/2} (\tilde{\hbar}^2 + \tilde{E}_b)^3} - \frac{\tilde{\hbar}(\tilde{\hbar}^3 - (1 \mp \tilde{\hbar})\tilde{\hbar}\tilde{E}_b \pm \tilde{E}_b^2)(2\ln(-\tilde{E}_b) - \ln(\tilde{E}_b^2 - 4\tilde{\hbar}^2))}{4(\tilde{\hbar}^2 + \tilde{E}_b)^3}. \quad (54)$$

Note that, because $\langle 10 | \hat{G}_0(E_b, \mathbf{p}) | 00 \rangle = 0$, $N_{10} = 0$ for the case $\mathbf{P} = \mathbf{0}$.

References

- [1] Y.-J. Lin, K. Jiménez-García and I. B. Spielman, *Spin-orbit-coupled Bose-Einstein condensates*, Nature **471**, 83 (2011), doi:[10.1038/nature09887](https://doi.org/10.1038/nature09887).
- [2] J. Dalibard, F. Gerbier, G. Juzeliūnas and P. Öhberg, *Colloquium: Artificial gauge potentials for neutral atoms*, Rev. Mod. Phys. **83**, 1523 (2011), doi:[10.1103/RevModPhys.83.1523](https://doi.org/10.1103/RevModPhys.83.1523).
- [3] L. W. Cheuk, A. T. Sommer, Z. Hadzibabic, T. Yefsah, W. S. Bakr and M. W. Zwierlein, *Spin-injection spectroscopy of a spin-orbit coupled Fermi gas*, Phys. Rev. Lett. **109**, 095302 (2012), doi:[10.1103/PhysRevLett.109.095302](https://doi.org/10.1103/PhysRevLett.109.095302).
- [4] P. Wang, Z.-Q. Yu, Z. Fu, J. Miao, L. Huang, S. Chai, H. Zhai and J. Zhang, *Spin-orbit coupled degenerate Fermi gases*, Phys. Rev. Lett. **109**, 095301 (2012), doi:[10.1103/PhysRevLett.109.095301](https://doi.org/10.1103/PhysRevLett.109.095301).
- [5] R. J. Elliott, *Spin-orbit coupling in band theory—character tables for some "double" space groups*, Phys. Rev. **96**, 280 (1954), doi:[10.1103/PhysRev.96.280](https://doi.org/10.1103/PhysRev.96.280).

- [6] G. Dresselhaus, A. F. Kip and C. Kittel, *Spin-orbit interaction and the effective masses of holes in germanium*, Phys. Rev. **95**, 568 (1954), doi:[10.1103/PhysRev.95.568](https://doi.org/10.1103/PhysRev.95.568).
- [7] G. Dresselhaus, *Spin-orbit coupling effects in zinc blende structures*, Phys. Rev. **100**, 580 (1955), doi:[10.1103/PhysRev.100.580](https://doi.org/10.1103/PhysRev.100.580).
- [8] E. I. Rashba and V. I. Sheka, *Symmetry of energy bands in crystals of wurtzite type II. Symmetry of bands with spin-orbit interaction included*, Fiz. Tverd. Tela: Collected Papers **2**, 162–176 (1959), English translation available as supplementary material to Ref. [40].
- [9] R. Winkler, *Spin-Orbit Coupling Effects in Two-Dimensional Electron and Hole Systems*, Springer, Berlin (2003).
- [10] Z. Wu, L. Zhang, W. Sun, X.-T. Xu, B.-Z. Wang, S.-C. Ji, Y. Deng, S. Chen, X.-J. Liu and J.-W. Pan, *Realization of two-dimensional spin-orbit coupling for Bose-Einstein condensates*, Science **354**, 83 (2016), doi:[10.1126/science.aaf6689](https://doi.org/10.1126/science.aaf6689).
- [11] L. Huang, Z. Meng, P. Wang, P. Peng, S.-L. Zhang, L. Chen, D. Li, Q. Zhou and J. Zhang, *Experimental realization of two-dimensional synthetic spin-orbit coupling in ultracold Fermi gases*, Nat. Phys. **12**, 540 (2016), doi:[10.1038/nphys3672](https://doi.org/10.1038/nphys3672).
- [12] K. Martiyanov, V. Makhalov and A. Turlapov, *Observation of a two-dimensional Fermi gas of atoms*, Phys. Rev. Lett. **105**, 030404 (2010), doi:[10.1103/PhysRevLett.105.030404](https://doi.org/10.1103/PhysRevLett.105.030404).
- [13] P. Dyke, E. D. Kuhnle, S. Whitlock, H. Hu, M. Mark, S. Hoinka, M. Lingham, P. Hannaford and C. J. Vale, *Crossover from 2D to 3D in a weakly interacting Fermi gas*, Phys. Rev. Lett. **106**, 105304 (2011), doi:[10.1103/PhysRevLett.106.105304](https://doi.org/10.1103/PhysRevLett.106.105304).
- [14] W. Ong, C. Cheng, I. Arakelyan and J. E. Thomas, *Spin-imbalanced quasi-two-dimensional Fermi gases*, Phys. Rev. Lett. **114**, 110403 (2015), doi:[10.1103/PhysRevLett.114.110403](https://doi.org/10.1103/PhysRevLett.114.110403).
- [15] M. G. Ries, A. N. Wenz, G. Zürn, L. Bayha, I. Boettcher, D. Kedar, P. A. Murthy, M. Neidig, T. Lompe and S. Jochim, *Observation of pair condensation in the quasi-2D BEC-BCS crossover*, Phys. Rev. Lett. **114**, 230401 (2015), doi:[10.1103/PhysRevLett.114.230401](https://doi.org/10.1103/PhysRevLett.114.230401).
- [16] P. A. Murthy, I. Boettcher, L. Bayha, M. Holzmann, D. Kedar, M. Neidig, M. G. Ries, A. N. Wenz, G. Zürn and S. Jochim, *Observation of the Berezinskii-Kosterlitz-Thouless phase transition in an ultracold Fermi gas*, Phys. Rev. Lett. **115**, 010401 (2015), doi:[10.1103/PhysRevLett.115.010401](https://doi.org/10.1103/PhysRevLett.115.010401).
- [17] D. Mitra, P. T. Brown, P. Schauß, S. S. Kondov and W. S. Bakr, *Phase separation and pair condensation in a spin-imbalanced 2D Fermi gas*, Phys. Rev. Lett. **117**, 093601 (2016), doi:[10.1103/PhysRevLett.117.093601](https://doi.org/10.1103/PhysRevLett.117.093601).
- [18] P. A. Murthy, M. Neidig, R. Klemt, L. Bayha, I. Boettcher, T. Enss, M. Holten, G. Zürn, P. M. Preiss and S. Jochim, *High-temperature pairing in a strongly interacting two-dimensional Fermi gas*, Science **359**, 452 (2018), doi:[10.1126/science.aan5950](https://doi.org/10.1126/science.aan5950).
- [19] K. Hueck, N. Luick, L. Sobirey, J. Siegl, T. Lompe and H. Moritz, *Two-dimensional homogeneous Fermi gases*, Phys. Rev. Lett. **120**, 060402 (2018), doi:[10.1103/PhysRevLett.120.060402](https://doi.org/10.1103/PhysRevLett.120.060402).

- [20] C. J. Vale and M. Zwierlein, *Spectroscopic probes of quantum gases*, Nat. Phys. **17**, 1305 (2021), doi:[10.1038/s41567-021-01434-6](https://doi.org/10.1038/s41567-021-01434-6).
- [21] M. Sato and Y. Ando, *Topological superconductors: a review*, Rep. Prog. Phys. **80**, 076501 (2017), doi:[10.1088/1361-6633/aa6ac7](https://doi.org/10.1088/1361-6633/aa6ac7).
- [22] C. Zhang, S. Tewari, R. M. Lutchyn and S. Das Sarma, *$p_x + ip_y$ superfluid from s -wave interactions of fermionic cold atoms*, Phys. Rev. Lett. **101**, 160401 (2008), doi:[10.1103/PhysRevLett.101.160401](https://doi.org/10.1103/PhysRevLett.101.160401).
- [23] J. D. Sau, R. M. Lutchyn, S. Tewari and S. Das Sarma, *Generic new platform for topological quantum computation using semiconductor heterostructures*, Phys. Rev. Lett. **104**, 040502 (2010), doi:[10.1103/PhysRevLett.104.040502](https://doi.org/10.1103/PhysRevLett.104.040502).
- [24] J. Alicea, *Majorana fermions in a tunable semiconductor device*, Phys. Rev. B **81**, 125318 (2010), doi:[10.1103/PhysRevB.81.125318](https://doi.org/10.1103/PhysRevB.81.125318).
- [25] M. Sato, Y. Takahashi and S. Fujimoto, *Non-Abelian topological orders and Majorana fermions in spin-singlet superconductors*, Phys. Rev. B **82**, 134521 (2010), doi:[10.1103/PhysRevB.82.134521](https://doi.org/10.1103/PhysRevB.82.134521).
- [26] K. Thompson, J. Brand and U. Zülicke, *Chiral two-dimensional p -wave superfluid from s -wave pairing in the Bose-Einstein-condensate regime*, Phys. Rev. A **101**, 013613 (2020), doi:[10.1103/PhysRevA.101.013613](https://doi.org/10.1103/PhysRevA.101.013613).
- [27] T. Hartke, B. Oreg, N. Jia and M. Zwierlein, *Quantum register of fermion pairs*, [arXiv:2103.13992](https://arxiv.org/abs/2103.13992).
- [28] J. P. Vyasankere and V. B. Shenoy, *Bound states of two spin- $\frac{1}{2}$ fermions in a synthetic non-Abelian gauge field*, Phys. Rev. B **83**, 094515 (2011), doi:[10.1103/PhysRevB.83.094515](https://doi.org/10.1103/PhysRevB.83.094515).
- [29] J. P. Vyasankere and V. B. Shenoy, *Rashbons: properties and their significance*, New J. Phys. **14**, 043041 (2012), doi:[10.1088/1367-2630/14/4/043041](https://doi.org/10.1088/1367-2630/14/4/043041).
- [30] S. Yang, F. Wu, W. Yi and P. Zhang, *Two-body bound state of ultracold Fermi atoms with two-dimensional spin-orbit coupling*, Phys. Rev. A **100**, 043601 (2019), doi:[10.1103/PhysRevA.100.043601](https://doi.org/10.1103/PhysRevA.100.043601).
- [31] L. Dong, L. Jiang, H. Hu and H. Pu, *Finite-momentum dimer bound state in a spin-orbit-coupled Fermi gas*, Phys. Rev. A **87**, 043616 (2013), doi:[10.1103/PhysRevA.87.043616](https://doi.org/10.1103/PhysRevA.87.043616).
- [32] X. Y. Yin, S. Gopalakrishnan and D. Blume, *Harmonically trapped two-atom systems: Interplay of short-range contact interaction and spin-orbit coupling*, Phys. Rev. A **89**, 033606 (2014), doi:[10.1103/PhysRevA.89.033606](https://doi.org/10.1103/PhysRevA.89.033606).
- [33] L. He and X.-G. Huang, *BCS-BEC crossover in 2D Fermi gases with Rashba spin-orbit coupling*, Phys. Rev. Lett. **108**, 145302 (2012), doi:[10.1103/PhysRevLett.108.145302](https://doi.org/10.1103/PhysRevLett.108.145302).
- [34] P. Zhang, L. Zhang and W. Zhang, *Interatomic collisions in two-dimensional and quasi-two-dimensional confinements with spin-orbit coupling*, Phys. Rev. A **86**, 042707 (2012), doi:[10.1103/PhysRevA.86.042707](https://doi.org/10.1103/PhysRevA.86.042707).

- [35] S. Takei, C.-H. Lin, B. M. Anderson and V. Galitski, *Low-density molecular gas of tightly bound Rashba-Dresselhaus fermions*, Phys. Rev. A **85**, 023626 (2012), doi:[10.1103/PhysRevA.85.023626](https://doi.org/10.1103/PhysRevA.85.023626).
- [36] Z. Fu, L. Huang, Z. Meng, P. Wang, L. Zhang, S. Zhang, H. Zhai, P. Zhang and J. Zhang, *Production of Feshbach molecules induced by spin-orbit coupling in Fermi gases*, Nat. Phys. **10**, 110 (2014), doi:[10.1038/nphys2824](https://doi.org/10.1038/nphys2824).
- [37] W. Ketterle and M. W. Zwierlein, *Making, probing and understanding ultracold Fermi gases*, Riv. Nuovo Cim. **31**, 247 (2008), doi:[10.1393/ncr/i2008-10033-1](https://doi.org/10.1393/ncr/i2008-10033-1).
- [38] C. J. Pethick and H. Smith, *Bose-Einstein Condensation in Dilute Gases*, Cambridge University Press, Cambridge, UK, 2nd edn. (2008).
- [39] Y. A. Bychkov and E. I. Rashba, *Properties of a 2D electron gas with lifted spectral degeneracy*, Pis'ma Zh. Eksp. Teor. Fiz. **39**, 66 (1984), [JETP Lett. **39**, 78 (1984)].
- [40] G. Bihlmayer, O. Rader and R. Winkler, *Focus on the Rashba effect*, New J. Phys. **17**, 050202 (2015), doi:[10.1088/1367-2630/17/5/050202](https://doi.org/10.1088/1367-2630/17/5/050202).
- [41] A. Manchon, H. C. Koo, J. Nitta, S. M. Frolov and R. A. Duine, *New perspectives for Rashba spin-orbit coupling*, Nat. Mater. **14**, 871 (2015), doi:[10.1038/nmat4360](https://doi.org/10.1038/nmat4360).
- [42] R. Winkler and U. Zülicke, *Discrete symmetries of low-dimensional Dirac models: A selective review with a focus on condensed-matter realizations*, ANZIAM J. **57**, 3 (2015), doi:[10.1017/S1446181115000115](https://doi.org/10.1017/S1446181115000115).
- [43] R. Eppenga and M. F. H. Schuurmans, *Effect of bulk inversion asymmetry on [001], [110], and [111] GaAs/AlAs quantum wells*, Phys. Rev. B **37**, 10923 (1988), doi:[10.1103/PhysRevB.37.10923](https://doi.org/10.1103/PhysRevB.37.10923).
- [44] L. Pricoupenko, *Isotropic contact forces in arbitrary representation: Heterogeneous few-body problems and low dimensions*, Phys. Rev. A **83**, 062711 (2011), doi:[10.1103/PhysRevA.83.062711](https://doi.org/10.1103/PhysRevA.83.062711).
- [45] P. Zhang, L. Zhang and Y. Deng, *Modified Bethe-Peierls boundary condition for ultracold atoms with spin-orbit coupling*, Phys. Rev. A **86**, 053608 (2012), doi:[10.1103/PhysRevA.86.053608](https://doi.org/10.1103/PhysRevA.86.053608).
- [46] J. Fuchs, C. Ticknor, P. Dyke, G. Veeravalli, E. Kuhnle, W. Rowlands, P. Hannaford and C. J. Vale, *Binding energies of ${}^6\text{Li}$ p-wave Feshbach molecules*, Phys. Rev. A **77**, 053616 (2008), doi:[10.1103/PhysRevA.77.053616](https://doi.org/10.1103/PhysRevA.77.053616).
- [47] A. Bergschneider, V. M. Klinkhamer, J. H. Becher, R. Klemt, G. Zürn, P. M. Preiss and S. Jochim, *Spin-resolved single-atom imaging of ${}^6\text{Li}$ in free space*, Phys. Rev. A **97**, 063613 (2018), doi:[10.1103/PhysRevA.97.063613](https://doi.org/10.1103/PhysRevA.97.063613).
- [48] M. Holten, L. Bayha, K. Subramanian, S. Brandstetter, C. Heintze, P. Lunt, P. M. Preiss and S. Jochim, *Observation of Cooper pairs in a mesoscopic 2D Fermi gas*, [arXiv:2109.11511](https://arxiv.org/abs/2109.11511).

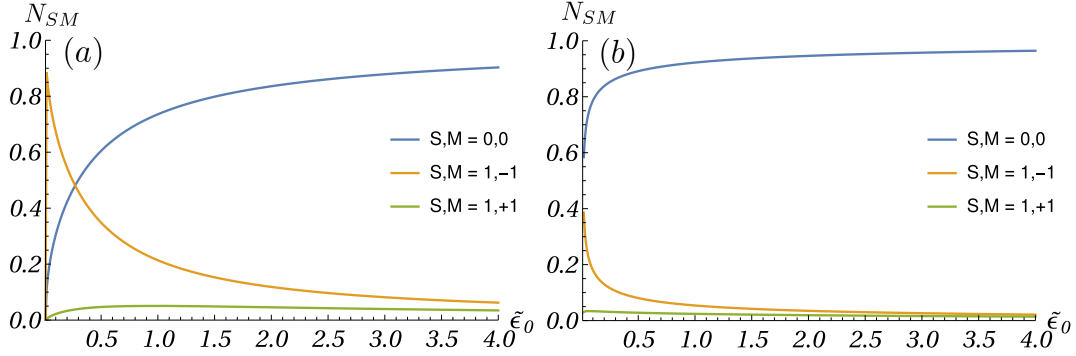


Figure 6: Fractional weights N_{SM} of total-spin eigenstates in the 2D-fermion bound state with zero COM momentum formed at fixed Zeeman energy $\tilde{h} = 1$, plotted as a function of the s -wave interaction strength parameterized by $\tilde{\epsilon}_0$ for 2D-type [panel (a)] and 1D-type [panel (b)] spin-orbit couplings. We do not show N_{10} as it vanishes identically in both cases for zero COM momentum.

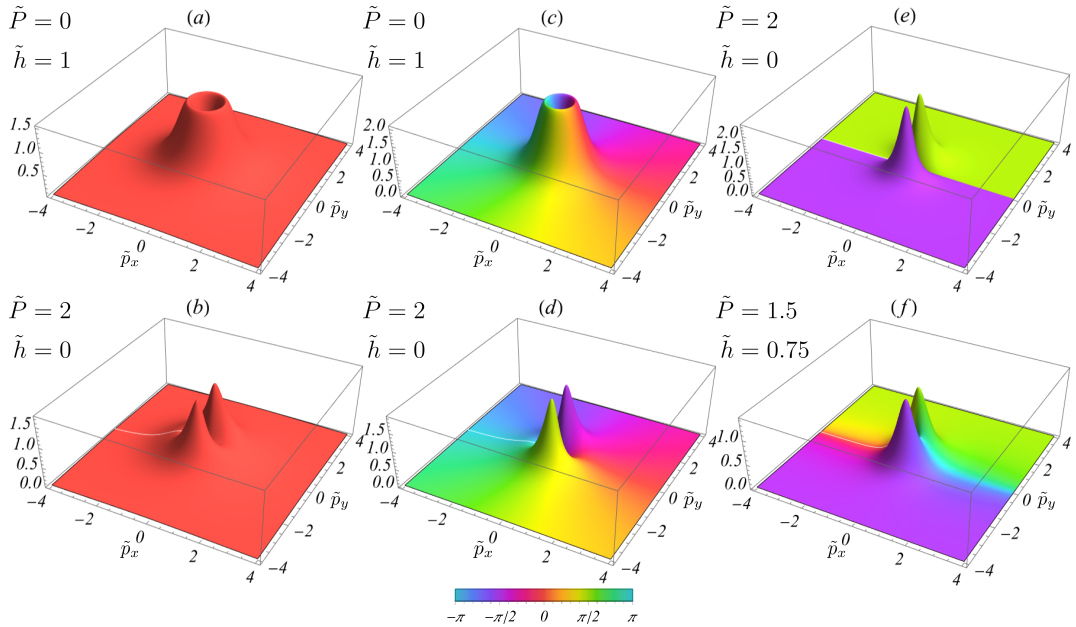


Figure 7: Orbital wave functions of the two-fermion bound state formed in the presence of 2D-Dirac spin-orbit coupling in relative-momentum $\mathbf{p} \equiv (p_x, p_y)$ representation. Surface height and color scale depict amplitude and phase, respectively, for $\langle SM | \psi_b(\mathbf{p}) \rangle / (c_P V_0) \equiv \langle SM | \hat{G}_P(E_b, \mathbf{p}) | 00 \rangle$. Panels (a) and (b) show the singlet component ($S = 0, M = 0$) and panels (c) and (d) the spin-polarized triplet component ($S = 1, M = -1$), which is dominant for $\mathbf{P} = \mathbf{0}$, $\tilde{h} \approx 1$ and weak s -wave interaction strength. Panels (e) and (f) show the spin-unpolarized triplet component ($S = 1, M = 0$), which occurs only for finite \mathbf{P} . The dimensionless interaction strength is $\tilde{\epsilon}_0 = 0.2$ and values of the Zeeman energy \tilde{h} and COM momentum $\mathbf{P}/(m\lambda) = (\tilde{P}, 0)$ as indicated in each panel.

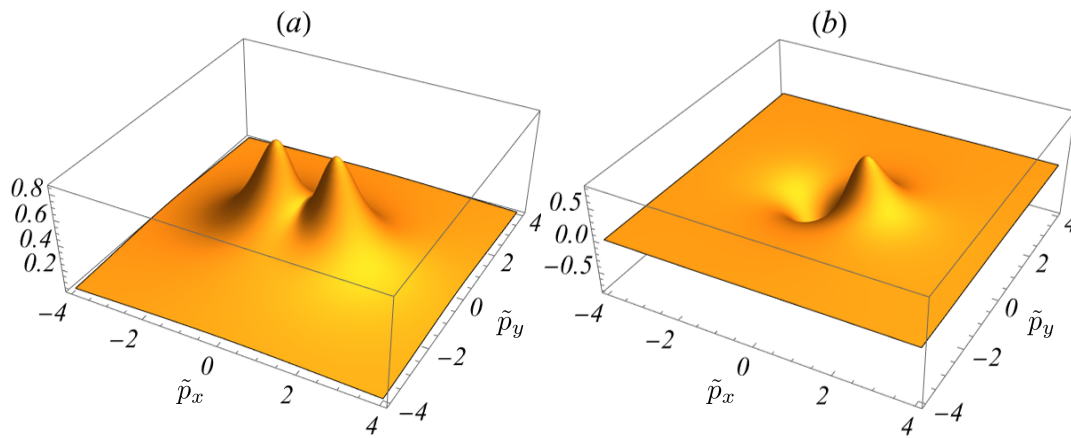


Figure 8: Orbital wave functions for two-fermion bound states formed in the presence of 1D-type spin-orbit coupling $\hat{\lambda}(\mathbf{p}) \equiv \lambda p_x \hat{\sigma}_x$ in the relative-momentum $\mathbf{p} \equiv (p_x, p_y)$ representation. Panel (a) shows the singlet $|00\rangle$ component and panel (b) the $|1 - 1\rangle$ triplet component. Surface plots show the real-valued functions $\langle SM|\psi_b(\mathbf{p})\rangle / (c_p V_0) \equiv \langle SM|\hat{G}_P(E_b, \mathbf{p})|00\rangle$, calculated with $\tilde{\epsilon}_0 = 0.01$ for the dimensionless interaction strength, Zeeman splitting $\tilde{h} = 1$ and vanishing COM momentum $\mathbf{P} = 0$.